Eur. Phys. J. C (2026) 86:222
https://doi.org/10.1140/epjc/s10052-026-15468-8

THE EUROPEAN PHYSICAL JOURNAL C

Regular Article - Theoretical Physics

The energy conditions and model selection in the local Universe

Namit Chandak[1], **Fulvio Melia**[2,a], **Jun-Jie Wei**[3,4]

[1] Department of Physics, The University of Arizona, Tucson, AZ 85721, USA
[2] Department of Physics, the Applied Math Program, and Department of Astronomy, The University of Arizona, Tucson, AZ 85721, USA
[3] Purple Mountain Observatory, Chinese Academy of Sciences, Nanjing 210023, China
[4] School of Astronomy and Space Sciences, University of Science and Technology of China, Hefei 230026, China

Received: 4 November 2025 / Accepted: 19 February 2026

Abstract The four principal energy conditions (ECs) in general relativity prohibit negative energies, repulsive gravity and superluminal energy flows. One must invoke exotic matter to violate any one of these, yet ΛCDM does so quite prominently during inflation and in the epoch of dark energy dominance. In this paper, we carry out model selection between the standard model and the $R_h = ct$ universe using a combination of HII galaxy and cosmic chronometer measurements in the local Universe, and directly compare the results to the constraints imposed by the ECs. We find that the latter cosmology is not only strongly favored by these data, with a likelihood of $\sim 92\%$ versus only $\sim 8\%$ for the former, but that its optimized fit is fully compliant with all four ECs, while ΛCDM's best fit violates the so-called strong energy condition at $z \lesssim 2$.

1 Introduction

Inflation was first proposed almost 50 years ago [1–4] to resolve several conflicts between the standard model, ΛCDM, and observations. The proposed accelerated expansion of the Universe was meant to solve major inconsistencies, including the temperature horizon problem, the spatial flatness in the cosmic spacetime, and the so-called monopole problem. Inflationary cosmology gradually became the standard picture, enjoying several notable successes, such as explaining the multi-peak structure in the angular power spectrum of the cosmic microwave background (CMB). It also accounted rather well for Baryonic Acoustic Oscillations and, perhaps to a lesser degree, the polarization of the CMB.

In this picture, dark energy in the guise of a cosmological constant accounts for the perceived current accelerated expansion of the Universe, while cold dark matter was chiefly responsible for the formation of large-scale structure. The scalar inflaton field, though, has never been directly observed, and its properties are inferred only weakly using an optimization of model parameters at much later times than the period ($\sim 10^{-35}$–10^{-34}s) when the exponentiated expansion was supposed to have occurred.

But the latest set of more precise cosmological measurements have begun to unravel this basic picture, which was largely constructed empirically based on poorly sampled data several decades ago. The newer observations from the Dark Energy Spectroscopic Instrument [5], the James Webb Space Telescope (JWST) [6–9], *Planck* [10,11], and even some older Hubble Space Telescope data [12], are at odds with the predictions of ΛCDM.

These measurements have revealed several significant challenges to the standard scenario, including: (i) The too early appearance of well-formed galaxies at $z > 14$ [13]. First identified by the Hubble Space Telescope at $z \sim 10$, this problem has been greatly exacerbated by the James Webb Space Telescope, which discovered galaxies up to $z \sim 17$. In the context of ΛCDM, these galaxies appear at ~ 230 Myr following the Big Bang, *before* the emergence of Pop III and Pop II stars at ~ 280 Myr; (ii) The discovery of supermassive black holes at redshifts approaching ~ 10 [14]. In the context of ΛCDM, these objects also would have started forming before the appearance of the earliest stars – and even the Big Bang. (iii) The formation and growth of Polycyclic Aromatic Hydrocarbon grains at redshifts ~ 7 that should have taken over a Gyr to form, yet were detected at ~ 500 Myr in ΛCDM [15]. Many of these conflicts are due to the same time compression problem in the standard model, i.e.,

Fulvio Melia: John Woodruff Simpson Fellow.

[a] e-mail: fmelia@email.arizona.edu (corresponding author)

Published online: 05 March 2026

an age of the Universe at $z > 6$ that is too short by about a factor 2.

The challenges faced by ΛCDM are not restricted to just the observations, however. Standard cosmology is also inconsistent with several fundamental physical principles in quantum mechanics, particle physics, and general relativity [16]. Each of them is a major hurdle on its own, but when viewed as a group they point to a need for a major overhaul of the standard theory [17,18]. An example of these is the electroweak horizon problem, in which ΛCDM cannot account for the fact that the Higgs vacuum expectation value is universal, beyond the causally connected regions in this standard scenario [19]. The electroweak symmetry would have been broken at $t \sim 10^{-11}$ s, well beyond the hypothesized inflationary transition at $t \sim 10^{-35}$ s, so this event creates a second horizon problem, independent of the CMB. We now know that the Higgs field is real and that its vacuum expectation value is universal, so the standard model is challenged strongly by this new evidence from particle physics. Similarly difficult challenges emerge from the cosmic initial entropy problem and the principle of equivalence, among several others summarized in Ref. [16].

The alternative Friedmann–Lemaître–Robertson–Walker (FLRW) cosmology known as the $R_h = ct$ universe not only fits the cosmological data better than the current standard model, but also eliminates all of its inconsistencies with fundamental physics [17,18]. By now the results of over 30 different types of comparative tests have appeared in the literature showing that the observations favour $R_h = ct$ over ΛCDM, often at a high level of confidence.

The mitigation of ΛCDM's inconsistencies includes: (i) providing a consistent timeline for the formation of large-scale structure at $z > 6$. In this model, the dark ages lasted until $\sim$ 830 Myr after the big bang, while the Epoch of Reionization persisted over the period $t \subset$ (830–1890) Myr. The 5–20 $M_\odot$ seeds that grew into high-z quasars were all formed after the transition between these two periods, consistent with the standard astrophysics of star formation in the early Universe; (ii) an elimination of the electroweak phase transition problem. In the $R_h = ct$ universe, regardless of when an event (like the electroweak phase transition) took place, the causally-connected regions always expanded to fill the entire visible Universe today [20]; (iii) a removal of the tension between the standard model's predictions and the latest measurements, based on the AGN Hubble diagram, high-z quasar Hubble diagram, the constancy of the cluster gas mass fraction, and so on. The Bayes Information Criterion applied to these tests typically favour the $R_h = ct$ universe with likelihoods exceeding $\sim$ 90–95%, compared to only $\sim$ 5–10% for the standard model.

At a fundamental level, the $R_h = ct$ universe is supported by several well-established constraints in our current physical theories. For example, its equation of state $p = -\rho/3$ for the total pressure p, in terms of the total energy density ρ in the cosmic fluid, is consistent with the zero active mass condition in general relativity, which is required for the validity of the FLRW ansatz [21]. As a result, this model does not need inflation to have fixed any inconsistencies in the early Universe. It also has no entropy problem, nor a monopole problem. And unlike the standard model, which violates at least one of the energy conditions from general relativity (both at high and low redshifts, as we shall see), $R_h = ct$ is completely consistent with all of the classical energy conditions at all times. And it must be said that $R_h = ct$ universe does all of this with just one free parameter – the Hubble Constant, H_0 – while ΛCDM struggles with as many as 11 or 12 parameters.

In this paper, we address one of the growing concerns with the standard model at low redshifts, stemming from its inconsistency with the well-established energy conditions in general relativity, which gave rise to the FLRW metric in the first place. We carry out a joint analysis of two independent data sets, HII galaxies and cosmic chronometers, and demonstrate that not only do the latest data strongly favour $R_h = ct$ over ΛCDM, but they do so satisfying the energy conditions in the former, while violating the so-called 'strong energy condition' (SEC) in the latter.

The HII galaxy catalog has now been extended to $z \sim 8$ by the latest JWST discoveries [22]. These sources serve as standard candles because their Hβ luminosity is correlated with the ionized gas velocity dispersion where the line radiation is produced. The relatively small scatter in these physical quantities is due to the fact that both the number of ionizing photons and the turbulent velocity of the gas increase with the mass of the starburst component. In their most recent analysis, Ref. [23] used this correlation to map the Hubble flow from redshift $\sim$ 0 to 7.5 in the context of flat-ΛCDM, corresponding to over 12 Gyr of cosmic expansion.

In a complementary fashion, luminous red galaxies known as cosmic chronometers provide us with a unique way of determining the universal expansion rate, $H(z)$, as a function of z. These measurements have been compiled by directly measuring the change in cosmic time as a function of redshift, which directly yields the Hubble Parameter. Galaxies with an age difference smaller than their evolutionary timescale provide the best cosmic chronometers, whose catalog now includes over 30 measurements [24,25].

These are the two independent data sets we shall combine for the joint analysis. Their selection is motivated in part by the facility with which the mathematical formalism of the energy conditions can be implemented to gauge whether or not the optimized fits are consistent with these general relativistic constraints. This is an area that has received very little attention thus far, but clearly needs to be explored more carefully going forward. We shall analyze these data and carry out model comparison, first by using each data set separately,

and then combining them for a joint study. As we shall see, the optimized parameters are not completely consistent in these three approaches, speaking to the possibility that the data aquisition may have missed some systematic error or simply underestimated the overall error in certain measurements. We shall also find, however, that all three approaches produce the same model selection outcome.

The four energy conditions require that : (i) a timelike observer always sees a non-negative energy density (the Weak Energy Condition, or WEC); (ii) the energy density is non-negative along a null vector, i.e., a four-vector whose time component is equal to the norm of its spatial components (the Null Energy Condition, or NEC); (iii) matter gravitates towards matter (the Strong Energy Condition, or SEC); and (iv) all energy and momentum fluxes are causal and oriented in the same way as the proper time of the observer (the Dominant Energy Condition, or DEC).

Together with the FLRW ansatz, these four energy conditions constrain various physical quantities, such as the pressure, density, the expansion rate and its time derivatives. With them, one can develop model independent bounds on the various quantities (see Eqs. 20–26 below). Some previous work along these lines has already appeared in the literature, including a demonstration that the standard model's interpretation of Type Ia supernovae clearly violates at least one of the energy conditions [26]. It has also been demonstrated that inflationary cosmology violates the energy conditions, while any basic scalar model of expansion in the early Universe based on the zero active mass condition does not [27].

This paper is structured as follows: in Sect. 2, we provide a brief theoretical basis for the FLRW metric and the general relativistic energy conditions applied to an FLRW universe. Following this, we present in Sect. 3 the mathematical constraints on the distance modulus and Hubble parameter in an expanding Universe. In Sect. 4, we describe the data and methodology, and we then report the optimization procedure and best fits for flat-ΛCDM and $R_{\rm h}{=}ct$ in Sects. 5 and 6. We end with a discussion in Sect. 7 and conclusion in Sect. 8.

2 Theoretical background

2.1 Friedmann–Lemaître–Robertson–Walker metric

We shall consider the specific application of the energy conditions to the local Universe, consistent with the Cosmological principle. The implied symmetries reduce the general spherically-symmetric ansatz of the spacetime metric to its Friedmann–Lemaître–Robertson–Walker (FLRW) form,

$$ds^2 = c^2\,dt^2 - a(t)^2\left[\frac{dr^2}{1-kr^2} + r^2\left(d\theta^2 + \sin^2\theta\,d\phi^2\right)\right], \tag{1}$$

in terms of the comoving coordinates (ct, r, θ, ϕ), the homogeneous expansion factor $a(t)$, and the spatial curvature constant, k. The observations are consistent with a spatially flat universe [11] so we shall adopt the value $k = 0$ throughout this paper.

Guided by the Cosmological principle, we also assume the perfect fluid approximation, in which the stress-energy tensor, $T_{\mu\nu}$, simplifies to

$$T^0_{\mu\nu} = u_\mu u_\nu(\rho + p)/c^2 - p g_{\mu\nu}, \tag{2}$$

in terms of the 4-velocity, u_μ, energy density, ρ, and pressure, p, in the fluid's rest frame. In a perfect fluid, there are no shear forces carrying momentum components in directions other than those associated with the components themselves [17]. In the comoving frame, $u_\mu = (c, 0, 0, 0)$, and so $T_{\mu\nu} = \mathrm{diag}(\rho, p, p, p)$. The energy density and pressure are given, respectively, as

$$\rho = \frac{3}{8\pi G}\left[\frac{\dot a^2}{a^2} + \frac{k}{a^2}\right], \tag{3}$$

$$p = -\frac{1}{8\pi G}\left[2\frac{\ddot a^2}{a^2} + \frac{\dot a^2}{a^2} + \frac{k}{a^2}\right], \tag{4}$$

where G is Newton's constant and the dots mean derivatives with respect to cosmic time.

Folding the FLRW metric in Eq. (1) through Einstein's field equation yields the Friedmann equation

$$H^2 \equiv \left(\frac{\dot a}{a}\right)^2 = \frac{8\pi G}{3c^2}\rho - \frac{kc^2}{a^2}, \tag{5}$$

the Raychaudhuri (or acceleration) equation [28],

$$\frac{\ddot a}{a} = -\frac{4\pi G}{3c^2}(\rho + 3p), \tag{6}$$

and the conservation of stress-energy,

$$\dot\rho = -3H(\rho + p). \tag{7}$$

It is always understood that ρ and p in these equations include all contributions from the cosmic fluid and the cosmological constant (if present), so a universe dominated by matter, radiation and Λ would be characterized by an energy density written as $\rho = \rho_{\rm m} + \rho_{\rm r} + \rho_\Lambda$, where $\rho_\Lambda \equiv c^4\Lambda/8\pi G$.

2.2 The energy conditions

The most recognizable application of the energy conditions in general relativity, especially after the awarding of the 2020 Nobel prize in physics to Sir Roger Penrose [29], are the singularity theorems (see also Refs. [30–33]). His seminal paper showed that null geodesics inside black holes are incomplete

whenever the Ricci tensor, $R_{\alpha\beta}$, satisfies the null convergence condition (with metric signature $[+,-,-,-]$)

$$R_{\mu\nu}k^\mu k^\nu \leq 0, \tag{8}$$

for any null vector k^μ. With this condition, even null geodesics inevitably encounter a termination point, or singularity.

Equation (8) is a geometric constraint, but Einstein's field equation translates it into a complementary constraint on $T^{\mu\nu}$ itself:

$$T_{\mu\nu}k^\mu k^\nu \geq 0, \tag{9}$$

given that $g_{\mu\nu}k^\mu k^\nu = 0$. This equation is known as the Null Energy Condition (NEC), that we now recognize as the first of several constraints on the energy in general relativity. Though the NEC was not used directly in the singularity theorems, it nevertheless represents a reasonable statement concerning the gravitational sources in $T_{\mu\nu}$ if the null convergence condition is real [34].

The energy conditions we describe here are derived within *classical* general relativity, and have been applied to the area increase theorem for black hole horizons [33], the topological censorship theorem [35], and the positive mass theorem [36]. They are violated somewhat by quantum effects [37], but these do not appear to be relevant to large classical systems, such as the cosmological spacetime.

Note, for example, that Penrose's [29] and Hawking and Ellis's [33] classical singularity theorem attesting to the existence of a Big Bang is based on the null convergence condition in Eq. (8), equivalent to the NEC in Eq. (9). It would be contradictory to maintain that such a constraint was required at $t = 0$, but not thereafter. Even so, a caveat to this argument is that quantum effects could have altered the dynamics of the Universe prior to the Planck time, eliminating the need for a singular beginning (see, e.g., Refs. [38,39]).

The pointwise energy conditions we use here restrict the form of $T^{\mu\nu}$ by ensuring that its contraction with two 4-vectors is never negative. This ensures that ρ must always be positive and that the flow of energy is never superluminal. The four most commonly used energy conditions are the following (see, e.g., Ref. [40]):

Weak energy condition (WEC): A timelike observer with 4-velocity u^μ must always see

$$T_{\mu\nu}u^\mu u^\nu \geq 0. \tag{10}$$

With a perfect fluid (Eq. 2), this condition is equivalent to the effective constraints

$$\begin{aligned} \rho &\geq 0 \\ \rho + p &\geq 0. \end{aligned} \tag{11}$$

So an observer with a timelike worldline always measures a non-negative total energy density. The pressure may be positive or negative but, if the latter, $|p|$ must never exceed ρ. The most concrete physical interpretation of this energy condition (see Eq. 7) is that the WEC prevents ρ from ever increasing as the Universe expands.

Null energy condition (NEC): This energy condition is similar to the WEC, except that the constraint on $T_{\mu\nu}$ is imposed on a null geodesic. The NEC condition is thus given in Eq. (9) which, for a perfect fluid, is equivalent to

$$\rho + p \geq 0. \tag{12}$$

Strong energy condition (SEC): The SEC emerges from the requirement that matter should gravitate towards matter, represented by a convergence constraint analogous to Eq. (8), except along the worldline of a timelike observer [41],

$$R_{\mu\nu}u^\mu u^\nu \leq 0. \tag{13}$$

Contracting Einstein's field equation with $g^{\mu\nu}$ yields the Ricci scalar

$$R = -\frac{8\pi G}{c^4}T, \tag{14}$$

in terms of the trace, $T \equiv T_{\mu\nu}g^{\mu\nu}$, of $T_{\mu\nu}$. Then Einstein's field equation may be written in the form

$$R_{\mu\nu} = -\frac{8\pi G}{c^4}\left(T_{\mu\nu} - \frac{1}{2}T g_{\mu\nu}\right), \tag{15}$$

allowing us to express the strong energy condition via the equation

$$\left(T_{\mu\nu} - \frac{1}{2}T g_{\mu\nu}\right)u^\mu u^\nu \geq 0. \tag{16}$$

Its effective representation for a perfect fluid is thus

$$\begin{aligned} \rho + p &\geq 0 \\ \rho + 3p &\geq 0. \end{aligned} \tag{17}$$

For the central theme in this paper, we point out that both null and timelike geodesics must converge to a point [33] in order for a singularity to emerge within the cosmic spacetime. Thus both Eqs. (8) and (13) must be satisfied. In other words, the existence of a Big Bang singularity requires the Universe to respect the SEC, not just the NEC. The latter is automatically satisfied when the SEC is also satisfied.

Dominant energy condition (DEC): Unlike the others, this condition encompasses two criteria: (i) the WEC and (ii) the energy and momentum fluxes must be causal and

orientated in the same way as the proper time of the observer. The resulting two constraints are therefore Eq. (10) and

$$T^{\mu}{}_{\nu}u^{\nu}T_{\mu}{}^{\alpha}u_{\alpha} \leq 0, \tag{18}$$

in which $-T^{\mu}{}_{\nu}u^{\nu}$ represents the 4-vector flux. With these constraints, the energy and momentum cannot be transported superluminally. In a perfect fluid, the DEC results in the constraints

$$\begin{aligned} \rho &\geq 0 \\ |p| &\leq \rho. \end{aligned} \tag{19}$$

2.3 Important caveats

There is still some debate concerning the validity of the classical energy conditions, almost always generated by the failure of favoured models and scenarios to fully satisfy them, including inflation, dark energy in the form of a cosmological constant, wormholes and warp drives. In truth, however, no unassailable evidence has ever emerged that any of the models or systems violating the energy conditions is unquestionably real or correct. Classical energy conditions assess the level of pathology in one's choice of stress-energy tensor, but their use is often reassessed, especially when they are violated.

Arguments questioning their validity tend to be specious and biased. At a fundamental level, the energy conditions are certainly based on strong physical intuition and sound theoretical justification. Take the NEC, for example. Its violation would point to the emergence of instabilities in the system [42,43] and superluminal propagation [44]. It has been argued that the NEC must be violated for wormholes to exist [45], or warp drives [46]. Conventional wisdom in cosmology maintains that the SEC must be violated in order for inflation to have occurred (see, e.g., Ref. [47]). The question, though, is why one should necessarily adopt the view that the energy conditions must be flawed rather than the opposite position – that a violation of the energy conditions argues against the validity and reality of pathological processes.

More dramatically, a violation of the WEC would spell catastrophe for the classical Universe because its vacuum would become unstable to the spontaneous separation of regions with positive and negative energy. What we do know for sure is that normal matter, e.g., baryons and non-baryons, and relativistic particles such as photons and neutrinos, all do satisfy every single standard energy condition.

Quantum effects do violate the classical energy conditions, but these do not appear to be relevant on a cosmic scale. For example, the most often used quantum argument against the classical energy conditions is based on the Casimir effect (see, e.g., Ref. [48]), in which the Casimir vacuum contains a negative energy density and thus violates all of the classical energy conditions.

But consider how this negative energy state is achieved. Quantum vacuum fluctuations of the electromagnetic field induce a small attractive force between two close parallel uncharged conducting plates. The classical energy conditions, however, are framed by the dynamical evolution of an *unbounded* vacuum, not the bounded system required to create the Casimir effect. The negative energy density in the Casimir vacuum results from the boundary conditions on the plates, quite unlike the unbounded dynamics underlying the classical energy conditions. One cannot scale the Casimir effect to a homogeneous and isotropic FLRW Universe because the required boundary conditions would violate the Cosmological principle.

Another argument raised against the validity of the energy conditions will actually feature very prominently in this paper. The optimized fitting of low-redshift data in the standard model, such as Type Ia supernovae, seems to suggest that the Universe is currently accelerating. That too violates the energy conditions. However, the existence of dark energy, which appears to be overwhelmingly supported by the data now, does not necessarily imply that the expansion is accelerating. It merely requires that the expansion not be decelerating. The comparative test we shall carry out below will directly address this very point, and our results will demonstrate that a non-accelerating expansion actually fits the low-redshift data better than the conventional ΛCDM. Thus, one cannot insist that the acceleration implied by the standard model argues against the validity of the energy conditions.

3 Constraints from the energy conditions

Writing the energy constraints in terms of the time derivatives of the expansion rate of the Universe using Eqs. (3) and (4), we get:

$$\textbf{NEC:} \quad -\frac{\ddot{a}}{a} + \frac{\dot{a}^2}{a^2} \geq 0, \tag{20}$$

$$\textbf{SEC:} \quad \frac{\ddot{a}}{a} \leq 0, \tag{21}$$

$$\textbf{WEC:} \quad \frac{\dot{a}^2}{a^2} \geq 0, \tag{22}$$

and

$$\textbf{DEC:} \quad -\frac{\dot{a}^2}{a^2} \leq -\frac{\ddot{a}}{a} \leq 2\frac{\dot{a}^2}{a^2}. \tag{23}$$

On integrating these once, we find that:

$$\textbf{NEC:} \quad \dot{a} \geq aH_0, \tag{24}$$

$$\textbf{SEC:} \quad \dot{a} \geq a_0H_0, \tag{25}$$

and

$$\textbf{DEC:} \qquad \dot{a} \leq \frac{a_0^3}{a^2} H_0. \tag{26}$$

3.1 EC bounds on the distance modulus

The luminosity distance $D_L(z)$, in terms of the acceleration of the Universe, is given by

$$D_L(z) = a_0(1+z)\, d(a), \tag{27}$$

where the comoving distance $d(a)$, for a flat universe, is given by

$$d(a) = \int_a^{a_0=1} \frac{1}{\dot{a}a} da. \tag{28}$$

Hence, the bounds on the distance modulus for different energy conditions using Eqs. (24)–(26), (27), (28) and (39) are

$$\textbf{NEC:}\ \mu(z) \leq 5\log_{10}\left[\frac{z(1+z)}{H_0}\right] + 25, \tag{29}$$

$$\textbf{SEC:}\ \mu(z) \leq 5\log_{10}\left[\frac{(1+z)}{H_0}\ln(1+z)\right] + 25, \tag{30}$$

$$\textbf{DEC:}\ \mu(z) \geq 5\log_{10}\left[\frac{(1+z)}{2H_0}\left(1 - \frac{1}{(1+z)^2}\right)\right] + 25. \tag{31}$$

3.2 EC bounds on the Hubble parameter

The bounds on the Hubble Parameter for different energy conditions using Eqs. (24)–(26) and (42) are

$$\textbf{NEC:}\ H \geq H_0, \tag{32}$$

$$\textbf{SEC:}\ H \geq H_0(1+z), \tag{33}$$

$$\textbf{DEC:}\ H \leq H_0(1+z)^3. \tag{34}$$

4 Observational data and methodology

4.1 HII galaxies

The data are taken from Ref. [23], including a full sample of 181 HIIGx analyzed in Ref. [49], 9 newer HIIGx from Ref. [50], and the 5 HIIGx newly discovered by JWST Ref. [22], constituting a total sample of 195 independently measured sources.

We calculate the Hβ luminosity from the reddening corrected Hβ fluxes, $F(\mathrm{H}\beta)$, and their 1σ uncertainties, as described in Ref. [51] (see also Ref. [52]):

$$L(\mathrm{H}\beta) = 4\pi D_L^2(z) F(\mathrm{H}\beta). \tag{35}$$

The most interesting of these sources are the high-redshift objects discovered recently by JWST. We list their corrected dispersions and 1σ uncertainties in column (3) of Table 1, along with the measured Hβ fluxes and their errors in column (4). The rest of the catalog may be found in Ref. [23] and references cited therein.

The emission-line luminosity is correlated with the ionized gas velocity dispersion, σ_v, [51,53,54] according to the ansatz

$$\log L(\mathrm{H}\beta) = \beta \log \sigma_v + \alpha\ , \tag{36}$$

where β is the slope and α is a constant representing the logarithmic luminosity at $\log \sigma_v = 0$. Note, though, that α and β are cosmology-dependent nuisance parameters, so they must be optimized simultaneously with the rest of the cosmological parameters (if any). Most cosmological measurements, most famously of Type Ia SNe, must be made in the context of a pre-selected model. The implied reliance on such so-called nuisance parameters is thus unavoidable. One must therefore carefully take into account that any optimized model parameters are therefore also dependent on these correlation variables. A particularly relevant example, as we shall see, is the Hubble constant, which will have different values in the models being compared. In other words, not all cosmological parameters can be measured in a model-independent way.

With Eqs. (35) and (36), the distance modulus may be written as

$$\mu_{\rm obs} = 2.5\left[\beta \log \sigma_v + \alpha - \log F(\mathrm{H}\beta)\right] - 100.2\ , \tag{37}$$

with a corresponding error ($\sigma_{\mu_{\rm obs}}$) found via error propagation,

$$\sigma_{\mu_{\rm obs}} = 2.5\left(\beta^2\sigma^2_{\log\sigma_v} + \sigma^2_{\log F}\right)^{1/2}\ , \tag{38}$$

in terms of the 1σ uncertainties, $\sigma_{\log\sigma_v}$ and $\sigma_{\log F}$, in $\log\sigma_v$ and $\log F(\mathrm{H}\beta)$, respectively.

This measured quantity will be compared with the theoretically predicted distance modulus,

$$\mu_{\rm th} \equiv 5\log\left[\frac{D_L(z)}{\rm Mpc}\right] + 25. \tag{39}$$

In ΛCDM, $D_L(z)$ is given as

$$D_L^{\Lambda\rm CDM}(z) = \frac{c}{H_0}\frac{(1+z)}{\sqrt{\mid \Omega_{\rm k} \mid}}\ \mathrm{sinn}\left\{\mid \Omega_{\rm k} \mid^{1/2} \times \int_0^z \frac{dz}{\sqrt{\Omega_{\rm m}(1+z)^3 + \Omega_{\rm k}(1+z)^2 + \Omega_{\rm de}(1+z)^{3(1+w_{\rm de})}}}\right\}, \tag{40}$$

Table 1 Flux and gas velocity dispersion of HII galaxies discovered by JWST[a]

Name	z	$\log \sigma_v$ (km s^{-1})	$\log F(\mathrm{H}\beta)$ (erg s^{-1} cm^{-2})
JADES-NS-00016745	5.56616 ± 0.00011	1.731 ± 0.016	-17.64 ± 0.21
JADES-NS-10016374	5.50411 ± 0.00007	1.785 ± 0.014	-18.14 ± 0.20
JADES-NS-00019606	5.88979 ± 0.00008	1.622 ± 0.019	-18.11 ± 0.27
JADES-NS-00022251	5.79912 ± 0.00007	1.621 ± 0.011	-17.86 ± 0.11
JADES-NS-00047100	7.43173 ± 0.00015	1.868 ± 0.024	-17.62 ± 0.39

[a] Taken from Ref. [23]

in terms of the energy density, $\rho = \rho_r + \rho_m + \rho_{\rm de}$, including radiation, matter (luminous and dark), and dark energy, expressed as fractions of today's critical density, $\rho_c \equiv 3c^2H_0^2/8\pi G$: $\Omega_m \equiv \rho_m/\rho_c$, $\Omega_r \equiv \rho_r/\rho_c$, and $\Omega_{\rm de} \equiv \rho_{\rm de}/\rho_c$. Also, $p_{\rm de} = w_{\rm de}\rho_{\rm de}$ is the dark-energy equation of state and Eq. (40) assumes negligible radiation pressure up to $z \sim 8$. In this paper, we assume spatial flatness throughout our analysis, so $\Omega_k = 0$ and the right side of this equation then reduces to $(1+z)c/H_0$ times the integral.

In the $R_{\rm h} = ct$ universe [55–58], we have instead

$$D_L^{R_{\rm h}=ct}(z) = \frac{c}{H_0}(1+z)\ln(1+z)\ . \tag{41}$$

4.2 Cosmic chronometers

The cosmic chronometers are a set of 34 mutually independent observations of galaxies which provide a measurement of the differential age of the Universe, avoiding possible problems with integrated histories over a period where the sources may be evolving. The expansion rate is inferred from

$$H(z) = \frac{\dot{a}}{a} = -\frac{1}{1+z}\frac{dz}{dt}. \tag{42}$$

For various reasons, the best cosmic chronometers are galaxies that evolve passively on a timescale much longer than their age difference. Observations indicate that the most massive galaxies contain the oldest stellar populations up to redshifts $z \sim 1$–2 [59–63]. More than 99% percent of the stellar mass in these massive galaxies formed at $z \geq 1$ [62,64]. In high-density regions (such as galaxy clusters), star formation terminated by redshift $z \sim 3$ [63], and other massive systems – those with stellar masses $5 \times 10^{11} M_\odot$ – concluded their star formation campaigns by $z \sim 2$ [65].

The empirical evidence suggests that galaxies in the highest density regions of clusters have been evolving passively since forming their stellar content at $z \geq 2$, without any subsequent chapters of star formation. One can therefore think of these galaxies as tracing the 'red envelope', hosting the oldest stars in the Universe at every redshift.

A direct way of determining the age of these galaxies is to use the 4000 Å break in its spectrum, which relates linearly

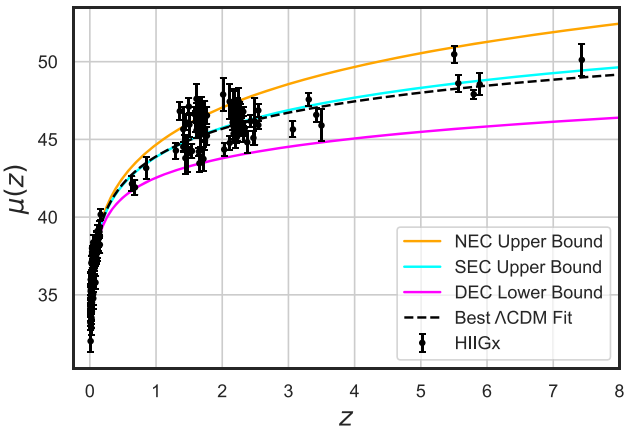

Fig. 1 Distance modulus for the HII galaxy data in the optimized, flat ΛCDM model. The violation of the SEC limit (blue curve) by the standard model prediction (dashed curve) becomes apparent in the redshift range $z \subset (0.2, 1.5)$, as highlighted by the magnified view in Fig. 2

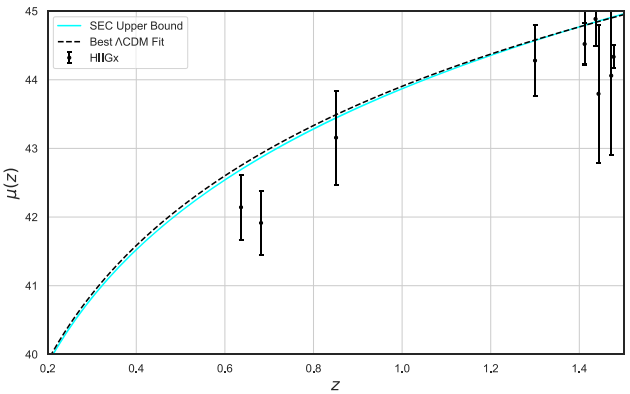

Fig. 2 The magnified region $z \subset (0.2, 1.5)$ from Fig. 1 where the SEC violation becomes apparent

to the age of old stellar populations [66]. This discontinuity of the spectral continuum is caused by metal absorption lines whose amplitude correlates linearly with the age and metal abundance. If the metallicity is known, then the difference in age between two galaxies is proportional to the difference in their 4000 Å amplitudes.

One must also be aware of the many systematic errors, however, that can bias this kind of analysis (see, e.g., Ref. [24]) like: (i) the degeneracy between the effect caused by a change in age and an effect due to a change in its stel-

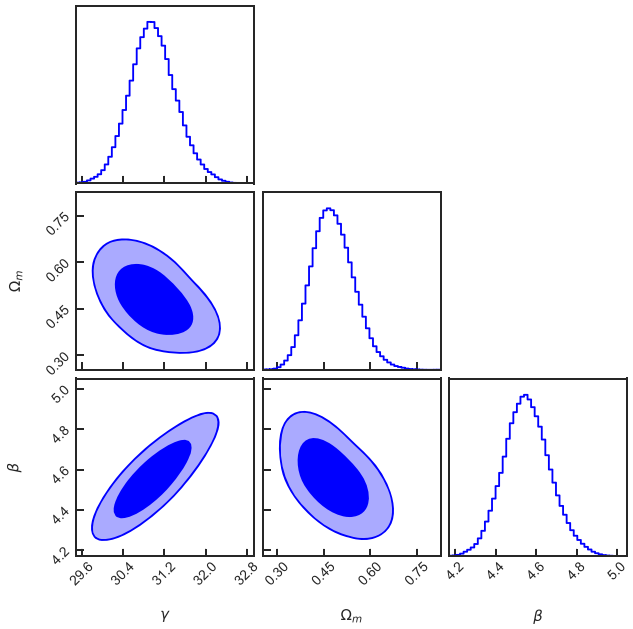

Fig. 3 1D probability distributions and 2D regions with the 1–2 σ contours corresponding to the parameters γ, $\Omega_{\rm m}$, and β in the flat ΛCDM fit (Fig. 1) to the HII galaxy data

lar metallicity; (ii) the choice of model for stellar population synthesis, being used to estimate the age or calibrate the 4000 Å break versus age relation leading to biasing in $H(z)$; and (iii) the possible existence of a progenitor bias [67], where the high-z samples of early-type galaxies might not be statistically equivalent to those at low redshifts.

Despite these caveats, one is motivated by the agreement between the results using different techniques. These data were assembled from the compilations of Refs. [25,68,69], over the redshift range $0 \leq z \leq 1.8$, providing a reasonably consistent picture of the universal expansion, especially when viewed with reference to theoretical expectations, that we consider in this work.

5 Best fit models

We carry out model selection comparing two distinct and unnested cosmologies, flat-ΛCDM and $R_{\rm h} = ct$, using a Maximizing Likelihood Estimate Procedure, utilizing a uniform prior for every parameter. The model parameters are optimized for each model and dataset. The optimizations are done using the Python Markov chain Monte Carlo (MCMC) module, EMCEE [70], and we discuss the results for each dataset and cosmological model in the following subsections.

5.1 Optimization using only HII galaxies

The coefficients α and β, and the cosmological parameters (H_0, and $\Omega_{\rm m}$ for ΛCDM and just H_0 for $R_{\rm h} = ct$) are optimized simultaneously using the 195 HIIGx objects, based on an implementation of Maximum Likelihood Estimation. The likelihood function is given by,

$$\mathcal{L}_{\rm HIIGx} = \prod_{i}^{195} \frac{1}{\sqrt{2\pi}\,\epsilon_{{\rm HIIGx},i}} \times \exp\left[-\frac{\left(\mu_{{\rm obs},i} - \mu_{\rm th}(z_i)\right)^2}{2\epsilon^2_{{\rm HIIGx},i}}\right], \tag{43}$$

where the variance on each HIIGx is given by,

$$\epsilon^2_{{\rm HIIGx},i} = \sigma^2_{\mu_{{\rm obs},i}} + \left[\frac{5\sigma_{D^{\rm th}_L,i}}{\ln 10\, D^{\rm th}_L(z_i)}\right]^2, \tag{44}$$

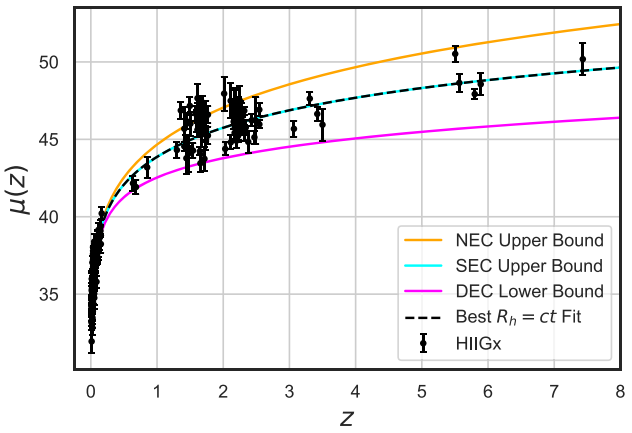

Fig. 4 Same as Fig. 1, except now for the $R_{\rm h} = ct$ universe. In this case, the SEC (blue) curve is identical to the model's prediction, so this cosmology is fully consistent with all of the energy conditions

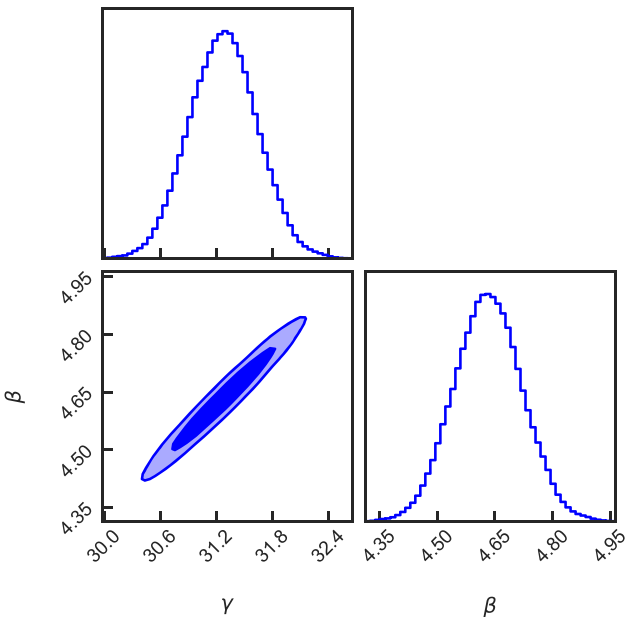

Fig. 5 1D probability distributions and 2D region with the 1–2 σ contours corresponding to the parameters γ, and β in the $R_{\rm h} = ct$ universe fit (Fig. 4) to the HII galaxy data

Table 2 Best-fitting results using solely the HII galaxy data

Model	γ	$\Omega_{\rm m}$	β	$-2\ln\mathcal{L}$	BIC	Probability
$R_{\rm h}=ct$	31.27 ± 0.36	–	4.63 ± 0.09	795.46	806.01	88.36%
ΛCDM	30.94 ± 0.44	0.48 ± 0.07	4.55 ± 0.11	794.24	810.06	11.64%

in terms of $\sigma_{D_L^{th},i}$ – the propagated uncertainty of $D_L^{\rm th}(z_i)$. Note that the first factor, $\epsilon_{\rm HIIGx}$, in Eq. (43) is not a constant, since it depends on the value of β. Thus, maximizing $\mathcal{L}$ is not exactly equivalent to minimizing the χ^2 statistic, i.e., $\chi^2=\sum_i \frac{(\mu_{{\rm obs},i}-\mu_{\rm th}(z_i))^2}{\epsilon^2_{{\rm HIIGx},i}}$. In addition, $-2\ln\mathcal{L}=\chi^2+\ln(2\pi\,\epsilon_{\rm HIIGx})$.

When using solely the HII galaxy data, the parameters H_0 and α are not independent, so we re-parameterize H_0 and α as follows:

$$\gamma=125.2-2.5\alpha-5\log H_0. \tag{45}$$

This re-parameterization becomes redundant when using the additional 36 HII sources in the 'anchor samples' (as used in Ref. [71]), since the luminosities assigned to this set constrain α and β individually. We are not including this sub-sample here because it is biased by the introduction of additional data not available to the rest of the HII galaxies in our sample. With the re-parameterization in (45), the likelihood function (43) takes the following form:

$$\mathcal{L}_{\rm HIIGx}=\prod_i^{195}\frac{1}{\sqrt{2\pi}\,\epsilon_{{\rm HIIGx},i}}\times\exp\left[-\frac{\Gamma_i^2}{2\epsilon^2_{{\rm HIIGx},i}}\right], \tag{46}$$

where,

$$\Gamma_i=2.5\left[\beta\log\sigma_{v,i}-\log F(H\beta)_i\right]-\gamma-5\log(H_0D_L^{th}[z_i]), \tag{47}$$

and the variance is still given by (44) since it does not depend on the Hubble constant H_0 or α.

5.1.1 ΛCDM

In the most basic ΛCDM model, $w_{\rm de}=-1$, leaving the two coefficients γ (re-parameterized from α and H_0 in Eq. 45) and β, and the matter density $\Omega_{\rm m}$ as the free parameters. The optimized fit is shown in Figs. 1 and 2, and the corresponding parameter values are presented in Table 2, with the 1–2 σ confidence regions plotted in Fig. 3.

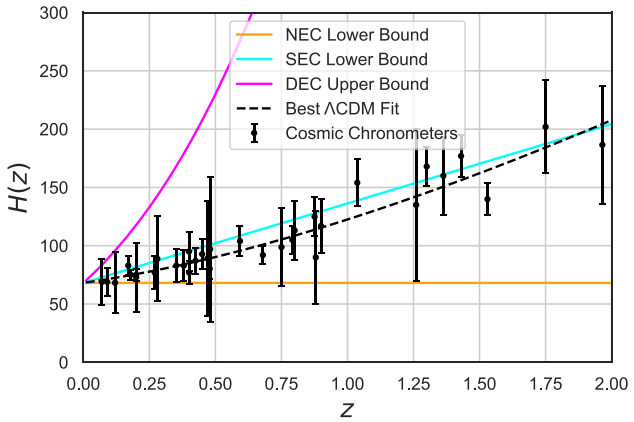

Fig. 6 The optimized flat-ΛCDM fit to the cosmic chronometer data. In this case, the violation of the SEC by the standard model can be seen within the redshift range $z\subset(0,1.75)$, confirming the result for the HII data in Figs. 1 and 2

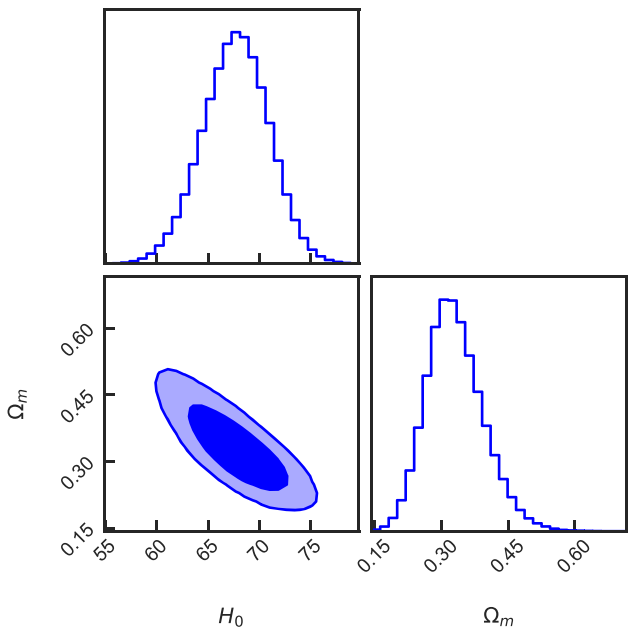

Fig. 7 1D probability distributions and 2D region with the 1–2 σ contours corresponding to the parameters H_0 and Ω_m in the flat-ΛCDM fit (fig. 6) to the cosmic chronometer data

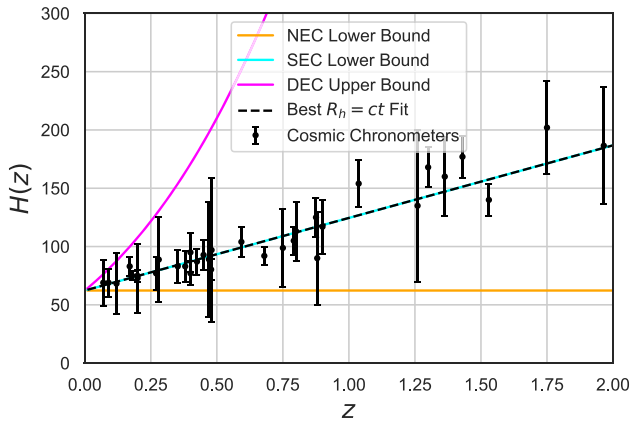

Fig. 8 Same as Fig. 6, except now for the $R_\mathrm{h} = ct$ universe. The SEC curve is identical to the model prediction in this cosmology, so the optimized fit to the cosmic chronometer data in $R_\mathrm{h} = ct$ satisfies all of the energy conditions

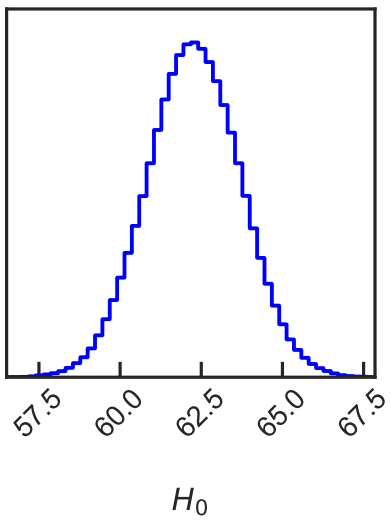

Fig. 9 1D probability distribution corresponding to the only parameter, H_0, in the $R_\mathrm{h} = ct$ universe fit (fig. 8) to the cosmic chronometer data

5.1.2 *The $R_\mathrm{h} = ct$ universe*

By comparison, the $R_\mathrm{h} = ct$ universe has only one free parameter, H_0, apart from the two coefficients α, and β, so after re-parameterization, the parameters to be optimized are γ, and β. The optimized fit is shown in Fig. 4, with the parameters listed in Table 2 and the 1–2 σ confidence regions shown in Fig. 5.

5.2 Optimization using only cosmic chronometers

Here, the cosmological parameters are optimized using the sample of 34 cosmic-chronometer measurements, with a

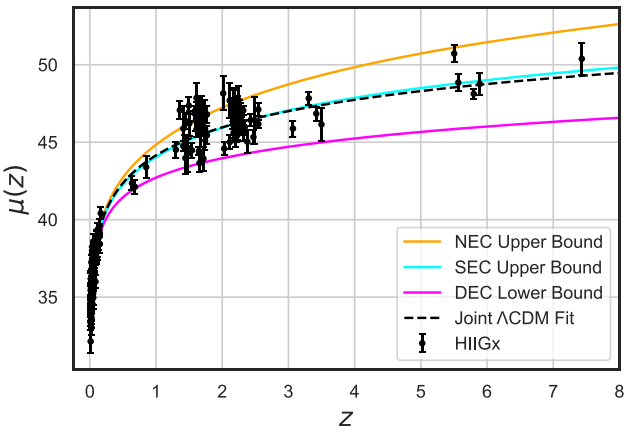

Fig. 10 The flat-ΛCDM fit to the HII galaxy data based on the maximum likelihood estimation of the parameters using the combined HII galaxy and cosmic chronometer measurements. The standard model's violation of the SEC, seen at intermediate redshifts in Figs. 1, 2 and 6, persists with the joint analysis

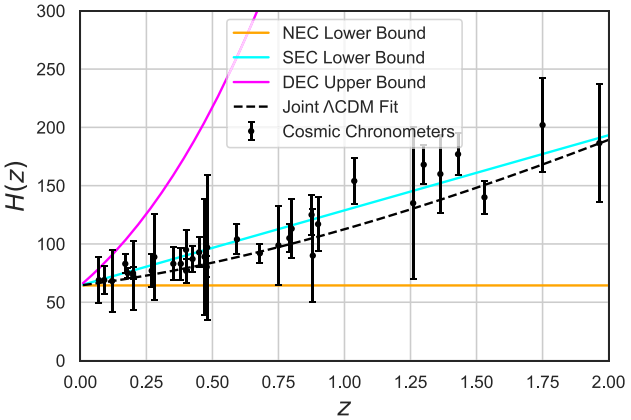

Fig. 11 The flat-ΛCDM fit to the cosmic chronometer data based on the maximum likelihood estimation of the parameters using the combined HII galaxy and cosmic chronometer data. Based on this joint optimization, the SEC violation by the standard model can again be seen at $z \subset (0, 2)$

Maximum likelihood Estimation given by

$$\mathcal{L}_\mathrm{cc} = \prod_i^{34} \frac{1}{\sqrt{2\pi}\,\epsilon_{\mathrm{cc},i}} \times \exp\left[-\frac{\left(H_{\mathrm{obs},i} - H_\mathrm{th}(z_i)\right)^2}{2\epsilon^2_{\mathrm{cc},i}}\right], \tag{48}$$

where the variance on each cosmic chronometer is given by

$$\epsilon^2_{\mathrm{cc},i} = \sigma^2_{H_{\mathrm{obs}},i}, \tag{49}$$

5.2.1 *ΛCDM*

For flat-ΛCDM, the 2 parameters optimized are H_0 and Ω_m, producing the fit shown in Fig. 6. The parameter values are

Table 3 Best-fitting results using solely the cosmic chronometers

Model	H_0 [km s^{-1} Mpc^{-1}]	$\Omega_{\rm m}$	$2\ln\mathcal{L}$	BIC	Probability
$R_{\rm h}=ct$	62.26 ± 1.42	–	277.86	281.38	65.87%
ΛCDM	67.72 ± 3.06	0.33 ± 0.06	275.65	282.70	34.13%

Table 4 Best-fitting results for the combined analysis of the HII galaxy and cosmic chronometer data

Model	H_0	$\Omega_{\rm m}$	α	β	$2\ln\mathcal{L}$	BIC	Probability
$R_{\rm h}=ct$	62.17 ± 1.42	–	33.98 ± 0.14	4.63 ± 0.09	1073.32	1089.62	92.32%
ΛCDM	64.26 ± 2.28	0.41 ± 0.05	33.96 ± 0.19	4.64 ± 0.11	1072.86	1094.59	7.68%

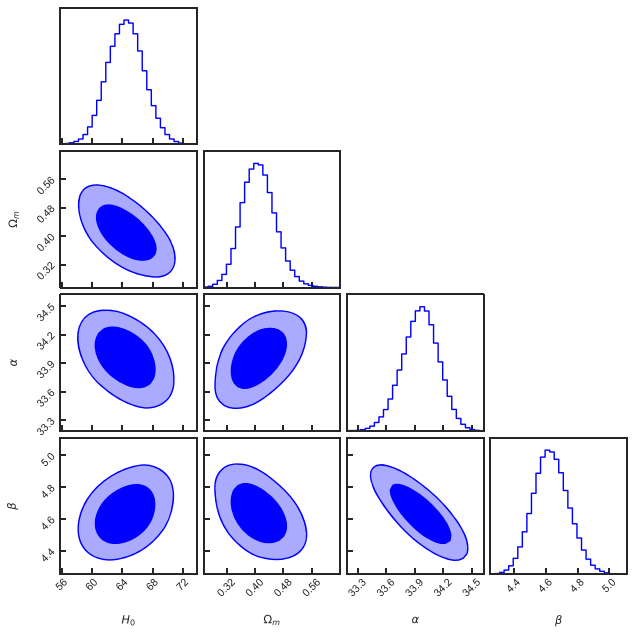

Fig. 12 1D probability distributions and 2D regions with the 1–2 σ contours corresponding to the parameters α, β, H_0, and Ω_m in the flat-ΛCDM joint fit (figs. 10 and 11) to the HII galaxy + cosmic chronometer data

listed in Table 3, with the 1–2 σ confidence regions shown in Fig. 7.

5.2.2 The $R_{\rm h}=ct$ universe

The $R_{\rm h}=ct$ universe has only one free parameter, H_0. The best fit curve is shown in Fig. 8, with the optimized parameter value listed in Table 3, and shown in Fig. 9.

6 Optimization using the combined data sets

The cosmological parameters and the coefficients α and β are optimized simultaneously using the 195 HIIGx and 34 cosmic chronometers based on the procedure outlined in §5, but with one change: we maximize the sum of the individual likelihoods using

$$\ln(\mathcal{L}_{\rm tot})=\ln(\mathcal{L}_{\rm HIIGx})+\ln(\mathcal{L}_{\rm cc}), \tag{50}$$

where $\mathcal{L}_{\rm HIIGx}$ and $\mathcal{L}_{\rm cc}$ are given by Eqs. (43) and (48), respectively.

6.1 ΛCDM

Again, we use the most basic ΛCDM model, optimizing the two coefficients, α and β, from the L-σ_v correlation, with H_0 and $\Omega_{\rm m}$ as the free cosmological parameters in this implementation. The joint best fit for the HII and cosmic chronometer data sets is shown in Figs. 10 and 11, respectively. The optimized parameter values corresponding to the optimized fit are presented in Table 4, with the 1–2 σ confidence regions shown in Fig. 12.

6.2 The $R_{\rm h}=ct$ universe

The $R_{\rm h}=ct$ universe has only one free cosmological parameter, H_0, apart from the two nuisance parameters characterizing the luminosity of the HII galaxies, α, and β, that must be optimized simultaneously with the Hubble constant. The best fit for this cosmology is shown in Figs. 13 and 14, while the optimized parameters are presented in Table 4 and the 1–2 σ confidence regions are shown in Fig. 15.

7 Discussion

The weak energy condition and the null energy condition imply timelike and null observers always see a non-negative energy density. A violation of any of these would allow the formation of infinite amounts of matter in finite regions of spacetime [33]. The dominant energy condition imposes the weak energy condition and causality of energy and momentum fluxes. A violation of the DEC would imply transfer of energy at speeds greater than that of light. Both, ΛCDM and $R_{\rm h}=ct$ satisfy these three ECs, based on the HII galaxy and

cosmic chronometer data we have analyzed in this paper (see Figs. 1, 4, 6, 8, 10, 11, 13, 14) The same is not true of the strong energy condition, however. This constraint requires that matter gravitates towards matter, i.e., that gravity is always attractive. In an FLRW universe, this implies that the cosmic expansion must never be accelerating, as stated mathematically in Eq. (21). The standard model violates this condition on two occasions. The first time during the postulated period of inflation [27]; the second during its predicted accelerated expansion of the Universe due to the dominance of a cosmological constant at low redshifts. This second instance of the SEC violation is manifested in Figs. 1, 2, 6, 10 and 11, which show that the best fit flat-ΛCDM cosmology requires the effects of antigravity to account for the data, regardless of whether we consider the HII galaxies and cosmic chronometers on their own, or whether we carry out a joint analysis. In sharp contrast, not only is the $R_{\rm h} = ct$ universe completely consistent with all four of the energy conditions, but it is also strongly favoured over flat-ΛCDM by the low-z measurements.

The Bayes Information Criterion (BIC) [72],

$$BIC = -2\ln\mathcal{L} + f\ln(n), \tag{51}$$

where $\ln\mathcal{L}$ is the maximized log likelihood, f is the number of free parameters, and n is the number of data points, is an asymptotic approximation to the outcome of Bayesian Inference (as $n \to \infty$). For the joint analysis, the BIC yields a probability of $\sim$ 92% versus only $\sim$ 8% for $R_{\rm h} = ct$ and flat-ΛCDM, respectively. The ΔBIC ≈ 5 for this model comparison suggests that the evidence in favour of the former model is therefore 'quite strong' (see Ref. [73] for a more detailed description of the BIC and other information criteria).

As we pointed out earlier, the Hubble parameter is cosmology-dependent. Its values determined by *Planck* (i.e., $= 67.4 \pm 0.5$ km s^{-1} Mpc^{-1}) [11], and that from Type Ia Supernovae ($= 73.04 \pm 1.04$ km s^{-1} Mpc^{-1}) [74] are based on the use of ΛCDM as the background cosmology. The value of H_0 optimized in $R_{\rm h} = ct$ is smaller (see, e.g., Table 4) than that in ΛCDM, but fully consistent with all previously optimized values using other data [18].

A second possible concern with this work is that the analysis of the HII galaxies and cosmic chronometers in flat-ΛCDM yields somewhat incompatible values for $\Omega_{\rm m}$ when using the data sets separately. Such a disagreement suggests that the data acquisition may not have been ideal, possibly missing some source of systematic uncertainty, or simply underestimating the overall error. The fact that some data points in Figs. 13 and 14 lie above (and below) the SEC Bound points to this possible underestimation. These data, however, have been used previously to test cosmological models and optimize their parameters, and the results we have obtained in this work are consistent with those earlier measurements. Quite reasonably, all three of the approaches we have taken for the analysis in this paper provide the same model selection outcome. The low-z data seem to favour the linear expansion predicted by $R_{\rm h} = ct$, which is also consistent with all four energy conditions from general relativity, over an accelerated expansion that violates the strong energy condition.

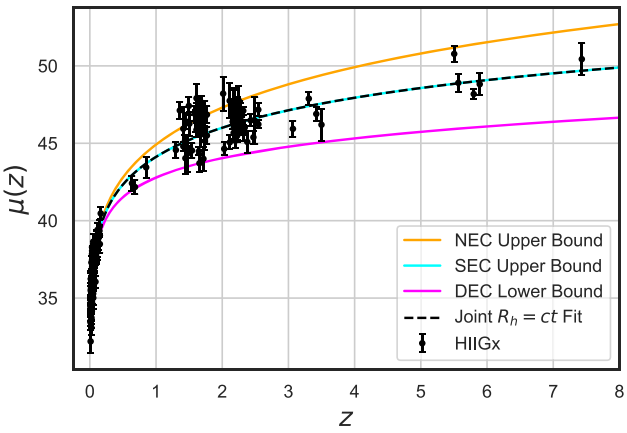

Fig. 13 Same as Fig. 10, except now for $R_{\rm h} = ct$. In this cosmology, the SEC is identical to the model's predicted $\mu(z)$, so all of the energy conditions are completely satisfied

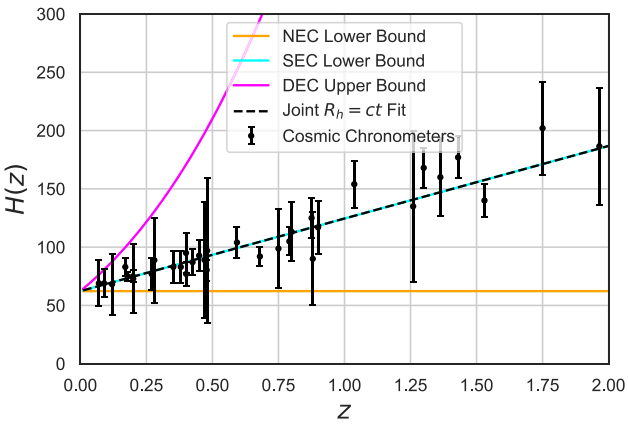

Fig. 14 Same as Fig. 11, except now for $R_{\rm h} = ct$. In this cosmology, the optimized fit to the cosmic chronometer data is fully consistent with all of the energy conditions

8 Conclusion

HII galaxies and cosmic chronometers have been used before for model selection among these two cosmologies [71,73,75], in each case producing an outcome favouring $R_{\rm h} = ct$. With the improvement in the source catalogues, these comparisons now favour this model even more robustly, particularly when using a joint analysis of the two data sets.

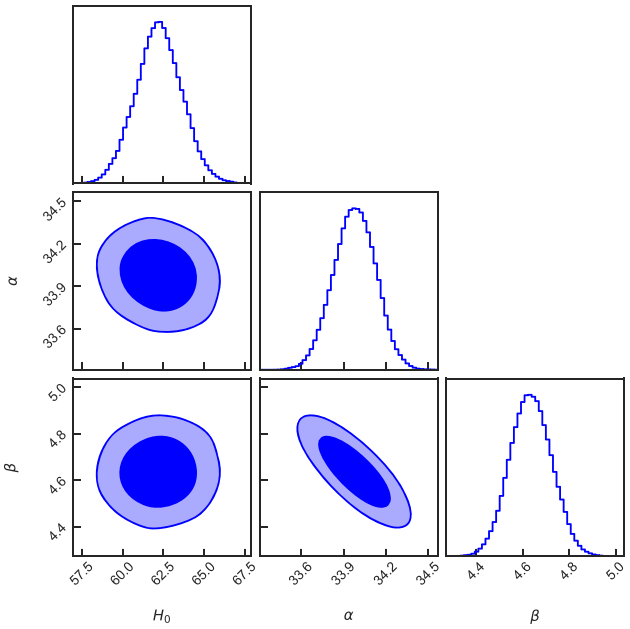

Fig. 15 1D probability distributions and 2D regions with the 1–2 σ contours corresponding to the parameters α, β, and H_0 in the $R_h = ct$ universe fit (figs. 13 and 14) to the combined HII galaxy + cosmic chronometer data

This in itself provides rather compelling evidence in favour of this model over the current standard scenario, but in this paper, we have also demonstrated that this comparison draws distinctly different perspectives within the framework of the energy conditions in general relativity. While ΛCDM violates at least one of these constraints at low redshifts, $R_h = ct$ is completely consistent with all of them.

This outcome, however, should not be viewed in isolation. It adds to the already large body of evidence favouring $R_h = ct$ over ΛCDM. And very interestingly, the inconsistency between the standard model and the energy conditions arises in several areas, most noticeably during the hypothesized inflationary expansion shortly after the Big Bang. Ironically, the supposed existence of the inflaton field is often touted as 'evidence' against the viability of the classical energy conditions. Yet the observations today are suggesting more and more that inflation is inconsistent with all of the available data, particularly the anisotropies in the CMB temperature field [76,77].

We suggest that one should therefore view the violation of the energy conditions by inflation as a compelling argument against its viability, a point that has been made more formally in Ref. [27]. Of course, inflation is not necessary in $R_h = ct$, which has no horizon problems and the fluctuations producing the large scale structure emerged naturally at the Planck scale [20,78].

The success of this analysis suggests that one ought to pay more attention to the energy conditions, not only in the very early Universe, but in the context of all cosmological observations, at both high and low redshifts.

Funding This work has no funding.

Data Availability Statement This manuscript has no associated data. [Author's' comment: No data were generated by this work.].

Code Availability Statement Code/software will be made available on reasonable request. [Author's comment: Code/software used in this study will be made available upon request.].

Funded by SCOAP[3].

References

1. A.A. Starobinskiĭ, Spectrum of relict gravitational radiation and the early state of the universe. Soviet JETP Lett. **30**, 682 (1979)
2. D. Kazanas, Dynamics of the universe and spontaneous symmetry breaking. ApJ Letters **241**, L59–L63 (1980)
3. A.H. Guth, Inflationary universe: A possible solution to the horizon and flatness problems. PRD **23**, 347–356 (1981)
4. A.D. Linde, A new inflationary universe scenario: A possible solution of the horizon, flatness, homogeneity, isotropy and primordial monopole problems. Phys. Lett. B **108**, 389–393 (1982)
5. D.E.S.I. Collaboration, A.G. Adame, J. Aguilar, S. Ahlen, S. Alam, G. Aldering, D.M. Alexander, R. Alfarsy, C.A. Prieto, M. Alvarez et al., The Early Data Release of the Dark Energy Spectroscopic Instrument. Astron. J. **168**, 58 (2024). arXiv:2306.06308
6. K.M. Pontoppidan, J. Barrientes, C. Blome, H. Braun, M. Brown, M. Carruthers, D. Coe, J. DePasquale, N. Espinoza, M.G. Marin et al., The JWST Early Release Observations. ApJ Letters **936**, L14 (2022). arXiv:2207.13067
7. S.L. Finkelstein, M.B. Bagley, P.A. Haro, M. Dickinson, H.C. Ferguson, J.S. Kartaltepe, C. Papovich, D. Burgarella, D.D. Kocevski, M. Huertas-Company et al., A Long Time Ago in a Galaxy Far, Far Away: A Candidate z $\sim$ 12 Galaxy in Early JWST CEERS Imaging. ApJ Letters **940**, L55 (2022). arXiv:2207.12474
8. T. Treu, G. Roberts-Borsani, M. Bradac, G. Brammer, A. Fontana, A. Henry, C. Mason, T. Morishita, L. Pentericci, X. Wang et al., The GLASS-JWST Early Release Science Program. I. Survey Design and Release Plans. ApJ **935**, 110 (2022). arXiv:2206.07978
9. S. Carniani, K. Hainline, F. D'Eugenio, D.J. Eisenstein, P. Jakobsen, J. Witstok, B.D. Johnson, J. Chevallard, R. Maiolino, J.M. Helton et al., Spectroscopic confirmation of two luminous galaxies at a redshift of 14. Nature **633**, 318–322 (2024). arXiv:2405.18485
10. P.A.R. Planck Collaboration, N. Ade, C. Aghanim, M. Armitage-Caplan, M. Arnaud, F. Ashdown, J. Atrio-Barandela, C. Aumont, A.J. Baccigalupi, P. Banday et al., results. XXII. Constraints on inflation. A&A **571**(2014), A22 (2013). arXiv:1303.5082

11. Planck Collaboration, N. Aghanim, Y. Akrami, M. Ashdown, J. Aumont, C. Baccigalupi, M. Ballardini, A. J. Banday, R. B. Barreiro, N. Bartolo, et al., Planck 2018 results. VI. Cosmological parameters, A&A **641**, A6 (2020). arXiv:1807.06209
12. P.A. Oesch, G. Brammer, P.G. van Dokkum, G.D. Illingworth, R.J. Bouwens, I. Labbé, M. Franx, I. Momcheva, M.L.N. Ashby, G.G. Fazio, V. Gonzalez, B. Holden, D. Magee, R.E. Skelton, R. Smit, L.R. Spitler, M. Trenti, S.P. Willner, A Remarkably Luminous Galaxy at z=11.1 Measured with Hubble Space Telescope Grism Spectroscopy. ApJ **819**, 129 (2016). arXiv:1603.00461
13. F. Melia, Strong observational support for the $R_h = ct$ timeline in the early universe. Physics of the Dark Universe **46**, 101587 (2024). arXiv:2407.15279
14. F. Melia, The cosmic timeline implied by the highest redshift quasars, ApJ Letters submitted (2024)
15. F. Melia, Strong Observational Support for the $R_h = ct$ Timeline in the Early Universe, Physics of the Dark Universe submitted (2024)
16. F. Melia, A Candid Assessment of Standard Cosmology. Pub Astron Soc Pacific **134**, 121001 (2022)
17. F. Melia, *The Cosmic Spacetime* (Taylor and Francis, Oxford, 2020)
18. F. Melia, *The Physics of Cosmology* (Elsevier, Amsterdam, 2026)
19. F. Melia, A solution to the electroweak horizon problem in the R_h=ct universe. European Physical Journal C **78**, 739 (2018). arXiv:1809.02885
20. F. Melia, A solution to the electroweak horizon problem in the Rh=ct universe. European Physical Journal C **78**, 739 (2018). arXiv:1809.02885
21. F. Melia, The Friedmann-Lemaître-Robertson-Walker metric. Mod. Phys. Lett. A **37**, 2250016 (2022)
22. A. de Graaff, H.-W. Rix, S. Carniani, K.A. Suess, S. Charlot, E. Curtis-Lake, S. Arribas, W.M. Baker, K. Boyett, A.J. Bunker et al., Ionised gas kinematics and dynamical masses of $z \gtrsim 6$ galaxies from JADES/NIRSpec high-resolution spectroscopy. A&A **684**, A87 (2024). arXiv:2308.09742
23. R. Chávez, R. Terlevich, E. Terlevich, A.L. González-Morán, D. Fernández-Arenas, F. Bresolin, M. Plionis, S. Basilakos, R. Amorín, M. Llerena, Mapping the Hubble flow from z∼0 to z∼7.5 with H II Galaxies. MNRAS **538**, 1264–1271 (2025). arXiv:2404.16261
24. M. Moresco, L. Verde, L. Pozzetti, R. Jimenez, A. Cimatti, New constraints on cosmological parameters and neutrino properties using the expansion rate of the Universe to z ∼175. JCAP **2012**, 053 (2012)
25. M. Moresco, A. Cimatti, R. Jimenez, L. Pozzetti, G. Zamorani, M. Bolzonella, J. Dunlop, F. Lamareille, M. Mignoli, H. Pearce et al., Improved constraints on the expansion rate of the Universe up to z∼1.1 from the spectroscopic evolution of cosmic chronometers. JCAP **2012**, 006 (2012). arXiv:1201.3609
26. J. Santos, J.S. Alcaniz, N. Pires, M.J. Rebouças, Energy conditions and cosmic acceleration. PRD **75**, 083523 (2007). (**astro-ph/0702728**)
27. F. Melia, Validation of the Numen Field by the Energy Conditions in the Early Universe. Ann. Phys. **535**, 2300157 (2023)
28. A. Raychaudhuri, Relativistic Cosmology. I. Phys. Rev. **98**, 1123–1126 (1955)
29. R. Penrose, Gravitational Collapse and Space-Time Singularities. PRL **14**, 57–59 (1965)
30. S.W. Hawking, The Occurrence of Singularities in Cosmology. II. Proc. R. Soc. Lond. Ser. A **295**, 490–493 (1966)
31. S.W. Hawking, The Occurrence of Singularities in Cosmology. III. Causality and Singularities. Proc. R. Soc. Lond. Ser. A **300**, 187–201 (1967)
32. S.W. Hawking, R. Penrose, The Singularities of Gravitational Collapse and Cosmology. Proc. R. Soc. Lond. Ser. A **314**, 529–548 (1970)
33. S.W. Hawking, G.F.R. Ellis, *The large-scale structure of space-time* (Cambridge University Press, 1973)
34. E. Curiel, A Primer on Energy Conditions, pp. 43–104. Springer, New York, New York, NY, (2017)
35. J.L. Friedman, K. Schleich, D.M. Witt, Topological censorship. PRL **71**, 1486–1489 (1993). arXiv:gr-qc/9305017
36. R. Schoen, S.-T. Yau, Positivity of the total mass of a general space-time. Phys. Rev. Lett. **43**, 1457–1459 (1979)
37. S.A. Fulling, *Aspects of Quantum Field Theory in Curved Space-time* (Cambridge University Press, 1989)
38. M. Visser, Scale anomalies imply violation of the averaged null energy condition. Phys. Lett. B **349**, 443–447 (1995). arXiv:gr-qc/9409043
39. J. Feldbrugge, J.-L. Lehners, N. Turok, No Smooth Beginning for Spacetime. PRL **119**, 171301 (2017). arXiv:1705.00192
40. E. Poisson, *A Relativist's Toolkit: The Mathematics of Black-Hole Mechanics* (Cambridge University Press, Cambridge, 2007)
41. P. Martín-Moruno, M. Visser, Classical and Semi-classical Energy Conditions. Fund. Theories Phys. **189**, 193 (2017). arXiv:1702.05915
42. S. Dubovsky, T. Grégoire, A. Nicolis, R. Rattazzi, Null energy condition and superluminal propagation. J. High Energy Phys. **2006**, 025 (2006). arXiv:hep-th/0512260
43. R.V. Buniy, S.D.H. Hsu, B.M. Murray, The null energy condition and instability. PRD **74**, 063518 (2006). arXiv:hep-th/0606091
44. F. Lobo, P. Crawford, Weak Energy Condition Violation and Superluminal Travel, in Current Trends in Relativistic Astrophysics (L. Fernández-Jambrina, L. M. González-Romero, eds.), **617**, p. 277. Springer, (2003)
45. M.S. Morris, K.S. Thorne, Wormholes in spacetime and their use for interstellar travel: A tool for teaching general relativity. Am. J. Phys. **56**, 395–412 (1988)
46. M. Alcubierre, LETTER TO THE EDITOR: The warp drive: hyper-fast travel within general relativity. Class. Quantum Gravity **11**, L73–L77 (1994). arXiv:gr-qc/0009013
47. E.-A. Kontou, K. Sanders, Energy conditions in general relativity and quantum field theory. Class. Quantum Gravity **37**, 193001 (2020). arXiv:2003.01815
48. T.A. Roman, Quantum stress-energy tensors and the weak energy condition. PRD **33**, 3526–3533 (1986)
49. A.L. González-Morán, R. Chávez, E. Terlevich, R. Terlevich, D. Fernández-Arenas, F. Bresolin, M. Plionis, J. Melnick, S. Basilakos, E. Telles, Independent cosmological constraints from high-z H II galaxies: new results from VLT-KMOS data. MNRAS **505**, 1441–1457 (2021). arXiv:2105.04025
50. M. Llerena, R. Amorín, L. Pentericci, A. Calabrò, A.E. Shapley, K. Boutsia, E. Pérez-Montero, J.M. Vílchez, K. Nakajima, Ionized gas kinematics and chemical abundances of low-mass star-forming galaxies at z ∼ 3. A&A **676**, A53 (2023). arXiv:2303.01536
51. R. Terlevich, E. Terlevich, J. Melnick, R. Chávez, M. Plionis, F. Bresolin, S. Basilakos, On the road to precision cosmology with high-redshift H II galaxies. MNRAS **451**, 3001–3010 (2015). arXiv:1505.04376
52. D. Calzetti, L. Armus, R.C. Bohlin, A.L. Kinney, J. Koornneef, T. Storchi-Bergmann, The Dust Content and Opacity of Actively Star-forming Galaxies. ApJ **533**, 682–695 (2000). arXiv:astro-ph/9911459
53. R. Chávez, E. Terlevich, R. Terlevich, M. Plionis, F. Bresolin, S. Basilakos, J. Melnick, Determining the Hubble constant using giant extragalactic H II regions and H II galaxies. MNRAS **425**, L56–L60 (2012). arXiv:1203.6222
54. R. Chávez, R. Terlevich, E. Terlevich, F. Bresolin, J. Melnick, M. Plionis, S. Basilakos, The L-σ relation for massive bursts of star formation. MNRAS **442**, 3565–3597 (2014). arXiv:1405.4010
55. F. Melia, *The edge of infinity. Supermassive black holes in the universe* (Cambridge University Press, Cambridge, 2003)

56. F. Melia, The cosmic horizon. MNRAS **382**, 1917–1921 (2007). arXiv:0711.4181
57. F. Melia, M. Abdelqader, The Cosmological Spacetime. International Journal of Modern Physics D **18**, 1889–1901 (2009). arXiv:0907.5394
58. F. Melia, A.S.H. Shevchuk, The R_h=ct universe. MNRAS **419**, 2579–2586 (2012). arXiv:1109.5189
59. J. Dunlop, J. Peacock, H. Spinrad, A. Dey, R. Jimenez, D. Stern, R. Windhorst, A 3.5-Gyr-old galaxy at redshift 1.55. Nature **381**, 581–584 (1996)
60. H. Spinrad, A. Dey, D. Stern, J. Dunlop, J. Peacock, R. Jimenez, R. Windhorst, LBDS 53W091: An Old, Red Galaxy at z = 1.552. ApJ **484**, 581–601 (1997). arXiv:astro-ph/9702233
61. L.L. Cowie, A. Songaila, A.J. Barger, Evidence for a Gradual Decline in the Universal Rest-Frame Ultraviolet Luminosity Density for Z<1. Astron. J. **118**, 603–612 (1999). arXiv:astro-ph/9904345
62. A. Heavens, B. Panter, R. Jimenez, J. Dunlop, The star-formation history of the Universe from the stellar populations of nearby galaxies. Nature **428**, 625–627 (2004). arXiv:astro-ph/0403293
63. D. Thomas, C. Maraston, R. Bender, C. Mendes de Oliveira, The Epochs of Early-Type Galaxy Formation as a Function of Environment. ApJ **621**, 673–694 (2005). arXiv:astro-ph/0410209
64. B. Panter, R. Jimenez, A.F. Heavens, S. Charlot, The star formation histories of galaxies in the Sloan Digital Sky Survey. MNRAS **378**, 1550–1564 (2007). arXiv:astro-ph/0608531
65. T. Treu, R.S. Ellis, T.X. Liao, P.G. van Dokkum, P. Tozzi, A. Coil, J. Newman, M.C. Cooper, M. Davis, The Assembly History of Field Spheroidals: Evolution of Mass-to-Light Ratios and Signatures of Recent Star Formation. ApJ **633**, 174–197 (2005). arXiv:astro-ph/0503164
66. M. Moresco, R. Jimenez, A. Cimatti, L. Pozzetti, Constraining the expansion rate of the Universe using low-redshift ellipticals as cosmic chronometers. JCAP **2011**, 045 (2011). arXiv:1010.0831
67. P.G. van Dokkum, M. Franx, The Fundamental Plane in CL 0024 at z = 0.4: implications for the evolution of the mass-to-light ratio. MNRAS **281**, 985–1000 (1996). arXiv:astro-ph/9603063
68. J. Simon, L. Verde, R. Jimenez, Constraints on the redshift dependence of the dark energy potential. PRD **71**, 123001 (2005). arXiv:astro-ph/0412269
69. D. Stern, R. Jimenez, L. Verde, S.A. Stanford, M. Kamionkowski, Cosmic Chronometers: Constraining the Equation of State of Dark Energy. II. A Spectroscopic Catalog of Red Galaxies in Galaxy Clusters. ApJ Supplements **188**, 280–289 (2010). arXiv:0907.3152
70. D. Foreman-Mackey, D.W. Hogg, D. Lang, J. Goodman, emcee: The MCMC Hammer. Pub Astron Soc Pacific **125**, 306 (2013). arXiv:1202.3665
71. J.-J. Wei, F. Melia, Model selection using the HII galaxy Hubble diagram. MNRAS **542**, L19–L23 (2025). arXiv:2506.04819
72. G. Schwarz, Estimating the Dimension of a Model. Ann. Stat. **6**, 461–464 (1978)
73. F. Melia, R.S. Maier, Cosmic chronometers in the $R_h = ct$ Universe. MNRAS **432**, 2669–2675 (2013). arXiv:1304.1802
74. A.G. Riess, W. Yuan, L.M. Macri, D. Scolnic, D. Brout, S. Casertano, D.O. Jones, Y. Murakami, G.S. Anand, L. Breuval, T.G. Brink, A.V. Filippenko, S. Hoffmann, S.W. Jha, W.D. Kenworthy, J. Mackenty, B.E. Stahl, W. Zheng, A Comprehensive Measurement of the Local Value of the Hubble Constant with 1 km s^{-1} Mpc^{-1} Uncertainty from the Hubble Space Telescope and the SH0ES Team. ApJ Letters **934**, L7 (2022). arXiv:2112.04510
75. J.-J. Wei, X.-F. Wu, F. Melia, The H II galaxy Hubble diagram strongly favours $R_h = ct$ over ΛCDM. MNRAS **463**, 1144–1152 (2016). arXiv:1608.02070
76. A. Ijjas, P.J. Steinhardt, A. Loeb, Inflationary paradigm in trouble after Planck 2013. Phys. Lett. B **723**, 261–266 (2013). arXiv:1304.2785
77. J. Liu, F. Melia, Viability of slow-roll inflation in light of the non-zero k_{min} measured in the cosmic microwave background power spectrum. Proc. R. Soc. Lond. Ser. A **476**, 20200364 (2020). arXiv:2006.02510
78. F. Melia, The $R_h = ct$ universe without inflation. A&A **553**, A76 (2013). arXiv:1206.6527